IJESRT

INTERNATIONAL JOURNAL OF ENGINEERING SCIENCES & RESEARCH TECHNOLOGY
EFFECT OF FRICTIONAL WELDING BETWEEN DIFFERENT STAINLESS-STEEL MATERIALS ON THERE IMPACT PROPERTIES

Azeen K. Mohammad*, Hawro Khalil
* Mechanical Department, College of Engineering, Salahaddin University-Erbil
Mechanical Department, College of Engineering, Salahaddin University-Erbil

ABSTRACT
The aim of the presented study was to investigate the effect of frictional welding between two different stainless steel materials on their impact properties. The study took two approaches; an experimental approach and a finite element analysis approach. Experimental approach was undertaken out to study the welded specimens' ability to withstand applied impact energy and to compare the results for speci¬mens welded with different forging pressures, 101.512MPa, 146.629MPa and 225.583MPa; non-welded specimens were also produced and tested. Finite element analysis approach was undertaken to study the generated heat during the process of welding and the heat transfer throughout the specimen as well as generating a heat transfer profile for the welding process.

KEYWORDS: Friction Welding, Impact Properties, Finite Element Analysis, Hardness, Heat Transfer.

INTRODUCTION
Friction welding obtained by frictional heat is a commercial process, which has found several applications with the advancement in technology; examples includes applications in automotive industry such as the manufacturing of valves, drive shafts and gear levers, applications in space parts industry such as radial pump pistons and drill bits, and other applications in which the of materials is required
  • either to obtain some desired properties of different materials.
  • or to overcome the difficulties of manufacturing single complicated parts.
  • or both.
without the concerns of typical welding failures[2], refer to [2] and [3] for more details on the applications of friction welding.

Friction welding is classified by the American Welding Society (AWS) as a solid state welding process that produces a weld at temperatures lower than the melting point of the base metals under compressive force contact of work pieces rotating or moving relative to one another, Figure 1, to produce heat and plastically displays material from the faying surfaces [4]. The resulting joint is of forged quality. Under normal conditions, the faying surfaces do not melt.

Even metal combinations not normally considered compatible can be joined by friction welding, such as aluminum to steel, copper to aluminum, titanium to copper and nickel alloys to steel, see Table1.As a rule, all metallic engineering materials which are forgeable can be friction welded, including automotive alloys, maraging steel, tool steel, alloy steels and tantalum. In addition, many castings, powder metals and metal matrix composites are weld-able[3].

Table 1: Weldable Combinations in Friction Welding

(Weldability matrix — rows and columns are the following materials: Aluminum, Aluminum Alloys, Brass, Bronze, Carbides Cemented, Cast Iron, Ceramic, Cobalt, Columbium, Copper, Copper Nickel, Iron Sintered, Lead, Magnesium, Magnesium Alloys, Molybdenum, Monel, Nickel, Nickel Alloys, Nimonic, Niobium, Niobium Alloys, Silver, Silver Alloys, Steel – Alloys, Steel – Carbon, Steel – Free Machining, Steel – Maraging, Steel – Sintered, Steel – Stainless, Steel – Tool, Tantalum, Thorium, Titanium, Titanium Alloys, Tungsten, Tungsten Carbide Cemented, Uranium, Vanadium, Valve Materials (Automotive), Zirconium Alloys.)

That being said, welded materials are subjected to changes in there mechanical and thermal properties due to the combined act of rubbing, heat generating, pressing, and forging. The highest rate of properties change is mostly found at the locations where the effect of the welding process is maximum, the welded faces, and drops with different rates proportionately to the distance from the welding zone as the effect of the welding process decays.

1.	Motor
2.	Brake
3.	Rotating Chuck
4.	Non Rotating Chuck
5.	Rotating Workpiece
6.	Non Rotating Workpiece
7.	Hydraulic Cylinder
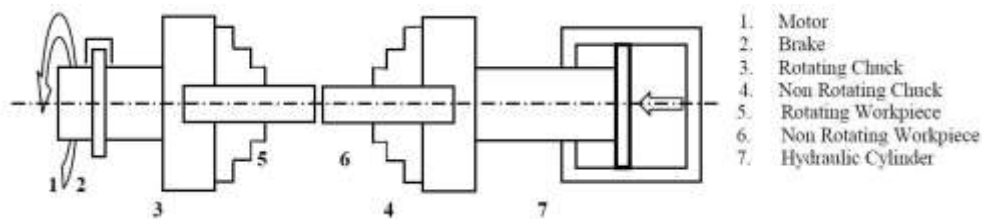
Figure 1: Layout of Continuous Drive Friction Welding [1]

The impact properties of the friction welded parts is one of the main limitations of such parts to be used in applications that include impact forces [5]. For this reason, the effect of the friction welding between different stainless-steel materials on the impact properties was investigated in this research.

The chemical composition was analyzed for both stainless-steels using a spectrometer. The analysis results for both materials, named α and β is shown in Table2 and Table3 respectively. Analysis result showed that the stainless-steel used was a martencite. Figure 2 and 3 shows the micro-structure imaging of both material.

Table 2: Spectrometer chemical composition for named α Stainless-Steel

	C	Si	Mn	P	S	Cr	Mo	Ni
	%	%	%	%	%	%	%	%
1	0.282	0.345	3.318	0.0100	0.0147	18.01	0.107	1.78
2	0.293	0.337	0.319	0.0094	0.0112	18.15	0.102	1.76
3	0.268	0.327	3.318	0.0096	0.0100	18.18	0.099	1.76
<x>(3)	0.281	0.337	0.318	0.0096	0.0120	18.11	0.102	1.77
sd	0.0124	0.0091	0.0004	0.0003	0.0024	0.090	0.0040	0.0134
rsd	4.4	2.7	0.1	3.0	20.3	0.5	3.9	0.8

	Al	Co	Cu	Nb	Ti	V	W	Fe
	%	%	%	%	%	%	%	%
1	0.0280	0.050	3.161	< 0.0020	0.0059	0.0199	0.130	78.73
2	0.0274	0.0500	3.166	< 0.0020	0.0057	0.0207	0.120	78.82
3	0.0238	0.051	3.167	< 0.0020	0.0055	0.0200	0.113	78.65
<x>(3)	0.0264	0.050	0.165	< 0.0020	0.0057	0.0202	0.121	78.67
sd	0.0023	0.0004	0.0032	0.0000	0.0002	0.0005	0.0089	0.057
rsd	8.7	0.8	1.9	0.0	2.7	2.3	7.4	0.1

Table 3: Spectrometer chemical composition for named β Stainless-Steel

	C	Si	Mn	P	S	Cr	Mo	Ni
	%	%	%	%	%	%	%	%
1	0.246	0.274	0.988	0.0074	0.0170	17.09	0.053	2.20
2	0.237	0.264	1.03	0.0058	0.0136	17.31	0.0495	2.17
3	0.209	0.261	1.03	0.0082	0.0133	17.33	0.0481	2.16
<x>(3)	0.230	0.266	1.02	0.0071	0.0148	17.24	0.050	2.17
sd	0.0195	0.0070	0.0244	0.0012	0.0024	0.131	0.0025	0.0209
rsd	8.5	2.6	2.4	16.0	16.3	0.8	4.9	1.0

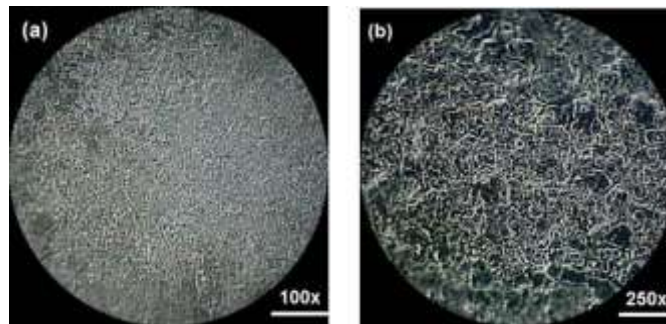|	Al	Co	Cu	Nb	Ti	V	W	Fe
	%	%	%	%	%	%	%	%
1	0.0122	0.0332	0.083	< 0.0020	0.0059	0.0324	< 0.0150	78.94
2	0.0105	0.0330	0.086	< 0.0020	0.0049	0.0293	< 0.0150	78.75
3	0.0048	0.0333	0.086	< 0.0020	0.0054	0.0282	< 0.0150	78.76
<x>(3)	0.0092	0.0332	0.085	< 0.0020	0.0054	0.0300	< 0.0150	78.82
sd	0.0039	0.0001	0.0016	0.0000	0.0005	0.0022	0.0000	0.105
rsd	42.7	0.4	1.9	0.0	9.2	7.2	0.0	0.1

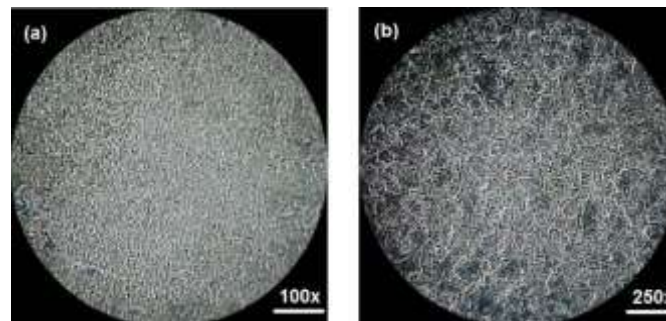*Figure 2: Micro-structure imaging of α Stainless-Steel*

Figure 3: Micro-structure imaging of β Stainless-Steel

SPECIMEN PREPARATION AND TESTING
Welding
Lath machine, Figure 4, was used for the welding process of prepared cylindrical rods, such approach is widely used due to the convenient and simplicity in addition to the controllability of friction pressure, timing and duration

[6][7][8]. One rod was fixed at the non-rotary end and the other was fixed at the rotary end. The non-rotary end has one degree of freedom of moving parallel to the rod's axis of rotation, this movement was manually controlled via screw type motion transmission allowing both motion and pressure control for that part. The rotary end has one degree of freedom of rotating about the rod's axis of rotation. the welding procedure was as follows,

1. Both rods ware tightly fixed as described above.
2. Both rods brought into contact by moving the non-rotary end toward the rotary end, the contact area at the faces to be welded together. The non-rotary end is manually forced to hold the friction pressure during the next step.
3. The rotary end is started, the rotation leads to friction at the contacted surfaces which increases there temperature rapidly.
4. As soon as visual surface redness is confirmed, indicating the temperature rising and the material being forge-able, the friction pressure changes into forging pressure by forcing the non-rotary end against the rotary end. Both surfaces start to forge into each other.
5. Upon visual confirmation of success forging, the rotary end is stopped first while maintaining the forging pressure until no redness is observed at the zone of welding.

Figure 4: Lathe Machine

For including the effect of different forging pressures in the study, welded joints were produced at three different forging pressures. The rotational speed, however, was maintained at 1030rpm for each welding process to reduce the number of variables in the study. Additionally, one specimen was produced, in the next section, without welding for each type of Stainless-Steel (i.e. α and β) for properties examination and evaluation of similar and dissimilar specimen; hence, the total number of specimens was 5. Table 4 includes the details of each weld.

Table 4: Friction welding parameters

Specimen No.	1	2	3
Friction Pressure	112.791	112.791	112.791
Friction time	30	30	30
Forging Pressure	101.512	146.629	225.583

Specimens Machining into Standard Dimensions
After the welded joints where obtained, milling machine was used to produce standard dimension impact test specimens, noting that no welding was required for α and β specimens. Figure 5 shows a schematic drawing of the specimens. Figure 6 shows the ready-to-test welded specimens.
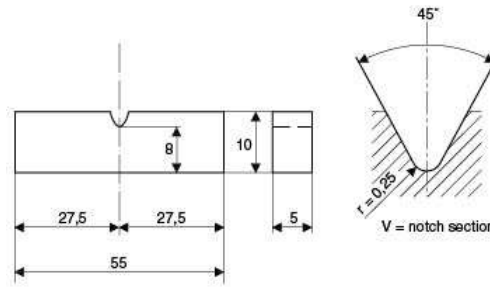
Figure 5: Charpy impact test specimen schematic drawing, dimensions in mm.

Figure 6: Charpy impact test specimens.

Testing

A manually operated laboratory Torsion-Test instrument was used. Figure 7 shows a schematic drawing of the charpy test instrument. The hammer is elevated manually and fixed at a height by a retractable fixing pin. when the specimen is in place, the pin is retracted and the hammer start to fall freely with a pendulum-like motion. As it reaches the impact point at the lowest level, the velocity of the hammer is maximized which, in terms, maximizes the energy of the hammer. Under these conditions, maximum impact force is applied on the specimen leading to fracture in the specimen. The impact energy is directly proportional to the mass of the hummer and the difference between initial and final height before the impact. The impact energy is constant for each instrument with constant height and hammer mass.
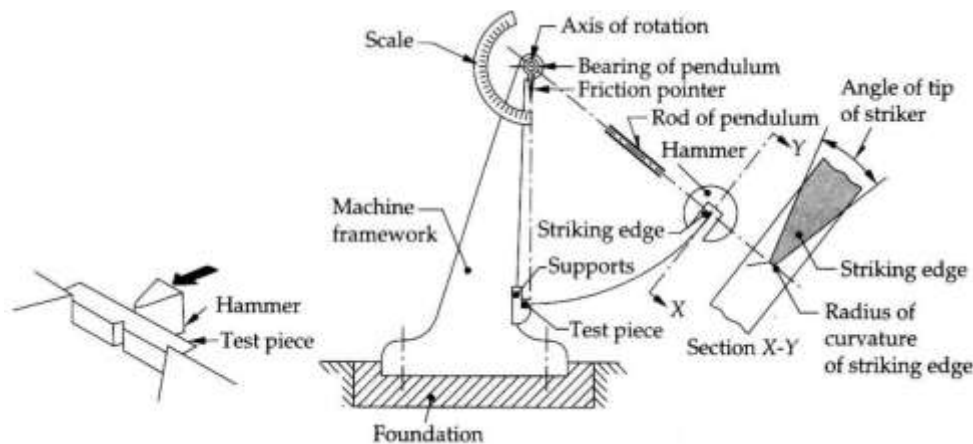

Figure 7: Charpy impact test instrument, schematic drawing.

The energy, required to fracture the specimen as adsorbed from the hammer. This amount of energy differs for each specimen depending on the mechanical properties of the specimen. The remaining energy in the hammer causes it to continue elevating after breaking the specimen. The final height which the hammer reaches is also directly proportional to the hammer's mass and the height difference after the impact.

Equation 1 shows the relation between the energy of an object, the mass and the height difference. The same equation applies before and after the impact. Having the mass of the hammer m and the gravitational acceleration g as constant, the energy required to fracture each specimen can be linked directly to the difference in height between the starting point of the hammer h_i, also a constant, and the ending point h_f of the hammer according to

Equation 4. This relation is used to read the remaining energy directly from a scale attached on the charpy instrument, linking the final height to the remaining energy to generate an energy scale for readings.[9]

$$\Gamma = mg(h_i - h_f) \tag{1}$$

Where:

Γ Energy gained or lost
m Mass
g Gravitational acceleration
h_i Initial hight
h_f Final hight
h_o Impact hight

Before Impact:

$$\Gamma_{\text{before}} = mg(h_i - h_o) \tag{2}$$

After Impact, remaining energy in the hammer:

$$\Gamma_{\text{after}} = mg(h_f - h_o) \tag{3}$$

Fracture Energy:

$$\Gamma_{\text{before}} - \Gamma_{\text{after}} = mg(h_i - h_o) - mg(h_f - h_o) \tag{4}$$
$$= mg[h_i - h_o - h_f + h_o] \tag{5}$$
$$= mg(h_i - h_f) \tag{6}$$

Having the exact same dimension for all specimens meant that calculating the stresses, which are found be relating the obtained energy readings and the specimen dimensions, was not necessary. For this study, that focuses on comparison rather than absolute values, the charpy readings were used as final results. It should be noticed that, to exclude the effect of air resistance, a test was carried out without specimen to measure the air resistance. The reading of the specimen free test was subtracted from each test readings before recording the final results, to count for the effect of the air resistance.

One concern of the impact test was the temperature of the specimens. Much research have been done on the relation between the temperature of materials and there mechanical properties. One mechanical property which has a direct effect on the impact energy absorbed by a material, and was a concern for this research, is the hardness of the material; other properties such as the ductility and the stress are also effected by the temperature. Researches has shown that the hardness of the material decreases when the temperature increase and the opposite is also true, the hardness increases as temperature decrees [10][11][12]. To exclude the effect of the temperature for all tests, the specimens had to be tested under the same material temperature. The selected temperature was 25°C which was obtained by placing each specimen in a controlled temperature bath for enough time to reach a steady state point at the selected temperature.

FINITE ELEMENT ANALYSIS SET-UP AND PROCEDURE
One of the major outcomes of the process of friction welding, which can't be practically monitored in real time, is the rising of temperature between the welded faces and the heat transfer through the specimen. The aim of rubbing both faces together is to generate heat as described before; therefore, a part of this study was concerned with how is the temperature generated and the heat is transferred within the specimen during the process of welding. To investigate that, DEFORM Ver.11 FEA tools were used to simulate the friction welding of Stainless-Steel and take a peek at the heat generation and transfer for the whole welded specimen. This method is commonly used when actual data monitoring is non-practical, Studies and Research based entirely on FEA can be found by referring to [13][14][15].

Modeling
DEFORM 3D modeling was used to generate the models, two cylindrical models of the same dimension (24mm diameter and 60mm height) and same assigned material, martensitic Stainless-Steel. Using 3D models, instead of 2D models, significantly increased the simulation time; however, the 3D models provided much better approximated heat transfer profile for the welding process and gave a three dimensional scoop of the heat generation within the specimens.

Meshing
As the main aim of this part of the study was to investigate the heat generation and transfer for the whole parts, it was decided that all nodes in the mesh are of equal concern. For this case, equal mesh size was used along with

fixed number of elements to uniformly mesh the specimens. Table 5 lists the meshing parameter. The meshed model for one half of the welded joint is shown in figure 8, a small error is introduced to the dimensions after meshing. This error is often encountered in FEA meshing and is negligible in amount for the purpose of this study, it rises from the attempt to split the entire part into the required amount of meshing elements.

Table 5: Model Mesh parameters

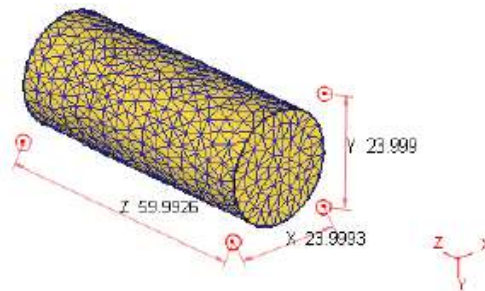| Detailed Settings	Remesh criteria	Summery
Type: System Setup Size Ratio: 1	Interference Depth: 0.7 Relative Remeshing Method: Global Remeshing	Number of Elements: 8000 Number of Nodes: 1599 Surface Polygons: 1682

Figure 8: One half meshed model

Movement and Boundary Conditions
Two tools were used in DEFORM to define motion and force applied to objects, movements and boundary conditions. Using the boundary conditions, one half of each of the modeled welded joints was fixed by adding a velocity boundary condition of zero in all directions, X, Y and Z. This was only applied to the lower end of this half, where no friction is presented and no movement is expected.

The second half didn't had any motion restrains. For this part, a pressing force was applied to the upper end to simulate the friction pressure and the forging pressure. The aim of the FEA study is to visualize the heat transfer in the specimens; hence, via iteration over a scale of different values, a pressure value of $1.3MPa$ was used in the simulation. In general, it was found that changing the boundary condition and movement values will affect the time for generating the simulations profile, the rate of heat transfer profile or the stress distribution profile as examples.

The Movement tools were used to simulate the rotation of the rotating half over a period of time, a rotational speed of $1030rpm$ was defined as movement for the second half.

Simulation
The simulation was divided into two stages:
1. The first stage simulated the friction pressure without rotation, for a time lapse of $1sec$.
2. The second stage simulated the friction pressure + the rotational speed, the heating process for a time lapse of $10sec$.

Table 6 lists the simulation parameters:

Table 6: Simulation Parameters

Units	SI
Type	Lagrangian incremental
Mode	Deformation & Heat Transfer
Simulation steps	100 for stage 1, 1000 for stage 2 and 100 for stage 3
Step increment	$0.01sec/step$
Remesh criteria	0.7 Relative
Solver	Conjugate gradient
Iteration method	Direct iteration
Velocity and force error	Default

RESULTS AND DISCUSSION

Testing Results

Figure 9 plots the fracturing energy for each specimen. The test results showed that the non-welded specimens α and β recorded the highest and second to highest fracture energy respectively. Specimen α resisted an impact energy of 20.2*J* before fracture and specimen β resisted an impact energy of 19.7*J* before fracture.

The welded specimens had a much lower fracture energy. Specimen 1 with the lowest forging pressure, Table 4, recorded fracture energy of 5.7*J*, specimen 2 with the intermediate forging pressure recorded fracture energy of 5.2*J* and specimen 3 with the lowest forging pressure recorded a fracture pressure of 3*J*.
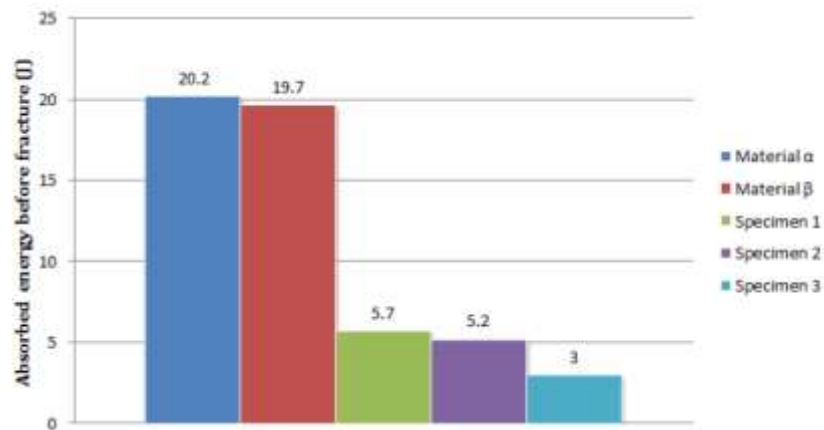

Figure 9: Fracture energy for the tested specimen

The cause for the considerable drop in the impact resistance for the welded materials, in additional to the difference between the obtained data for the non-welded specimens, is due to the change in the chemical composition at the welding area and its surrounding. The Welded specimen behaved as more brittle and less ductile materials comparing to the non-welded specimen. Also the dominance of this behaviour increases as the forging pressure increases.

Specimen α and β Results Discussion

Researches has been done on the effect of chemical composition of stainless-steels on their mechanical properties [16][17]. In general,

- **Carbon *C*:** An increased carbon concentration caused an increase in strength and a decrease in ductility.
- **Silicon *Si*:** A reduction in silicon caused an increase in ductility with little effect on strength.
- **Phosphorus *P*:** An increase in phosphorus caused an increase in rupture life and an improvement in ductility.
- **Boron *B*:** An increase in boron increased rupture life and ductility.

The chemical composition analysis for Stainless-Steel α and β, Table 2 and Table 3, should that both material contained Carbon, Silicon and Phosphorus, Boron was not presented in either material. Material α had higher amount of *C*, *Si* and *P* than material β with different percentages. This explains the difference between the test results for α Stainless-Steel and β Stainless-Steel. Having more carbon increased the hardness of α Stainless-Steel and the combined effect of Silicon and Phosphorus provided the ductility to withstand an impact up to the fracture energy, Figure 9. Having less carbon reduced the hardness of β Stainless-Steel and the same effect is addressed for Silicon and Phosphorus.

Welded Specimen 1, 2 and 3 Results Discussion

The welded specimens withstood much less impact energy before fracturing. This behaviour is related to the raising temperature during friction, the melting point of the presented elements and the forging pressures. The simulation results showed that the temperature rises to reach up to 2990 ºC, as described in the next section, at the rubbed surfaces. This temperature is above the melting point of most presented elements in material α and β. Table 7 list the melting point of each element that was counted for in the chemical composition analysis, Table 2 and 3

Page 3, in an descending order. Only Carbon and Tungsten has a higher melting point than 2990 ᵒC. This suggests that during the heating process, most of the elements presented in the welding zone will liquefy and form thin layers and spots of molten material which, in addition to other elements, includes the Silicon and the Phosphorus. The carbon might maintain its solid phase but becomes easier to forge due to the high temperature.

Table 7: Melting point of the presented elements in α stainless-steel and β stainless-steel

Element	Symbol	Melting Point deg C	Present in α	Present in β
Carbon	C	3500	0.281	0.32
Tungsten	W	3410	0.121	<0.0150
Molybdenum	Mo	2617	0.102	0.05
Niobium	Nb	2468	<0.002	<0.002
Vanadium	V	1890	0.0202	0.03
Chromium	Cr	1875	18.11	17.24
Titanium	Ti	1660	0.0057	0.0054
Iron	Fe	1535	78.67	78.82
Cobalt	Co	1495	0.05	0.0332
Nickel	Ni	1453	1.77	2.17
Silicon	Si	1410	0.337	0.266
Manganese	Mn	1245	0.318	1.02
Copper	Cu	1083	0.165	0.085
Aluminium	Al	660	0.0264	0.0092
Sulphur	S	113	0.012	0.0148
Phosphorus	P	44	0.0096	0.0071

When the contact faces are pressed one toward the other with the forging pressure, much of the molten element and less of carbon will be extruded out of the friction zone. Therefore, higher concentration of carbon will be presented at the friction zone and less concentrations of silicon and phosphorus. Increasing the concentration of carbon will increase the hardness but also decreases the ductility. Phosphorous has the lowest melting point which cause it to liquefy first and be extruded in higher percentage. Reduction in Phosphorous concentration reduces the rapture life and ductility. Silicon concentration will also be decreased and might cause an improvement in ductility. Overall, the effect of Carbon concentration increasing and Phosphorus concentration decreasing will dominate the effect of Silicon concentration decreasing.

This after welding composition will harden the specimen at the welding zone but weaken the ductility. The welded specimen will withstand less impact force before fracture at the welding zone due to the brittleness of that zone. Increasing the forging pressure will extrude more liquefied element from the welding zone and increase the concentration of carbon. For that reason, increasing the forging pressure will reduce the ductility and increases the brittleness. The reduction percentage in withstanding the impact force, in terms of energy, for the welded specimen 1, 2 and 3 comparing to the average of $19.95 J$ for the non-welded specimens was 71.42%, 92.72% and 96.76% respectively.

A magnified image of the fracture profile for each welded specimen is shown in Figure 10. The results indicate that the slop of the fracture profile increases as the forging pressure increases. This also means that the slop increases as the brittleness of the fractured zone increase. The fracture profile for each specimen was re-plotted from the same origin in Figure 11 for better vitalizing the different in the slops. Specimen 1, least brittle, had the smallest slop while specimen 3, the most brittle, had the largest slop.
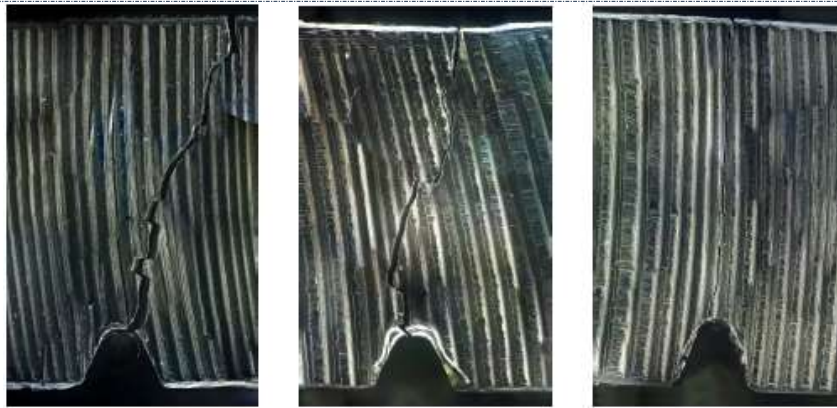
a) Specimen 1   b) Specimen 2   c) Specimen 3
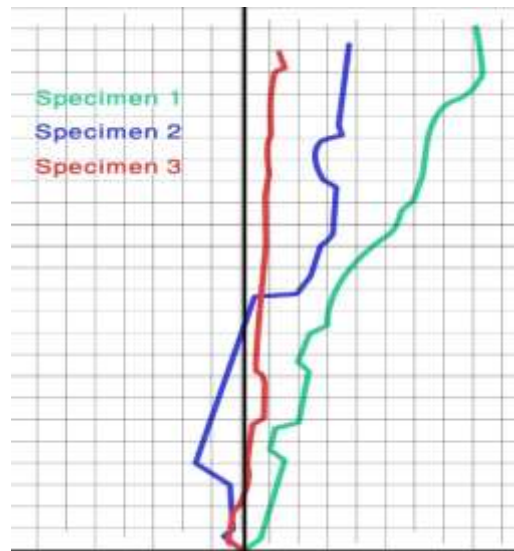*Figure 10: Magnified images of the fracture profiles.*

Figure 11: Welded specimens fracture profile plot.

Simulation Results

Finite Element Analysis was used to investigate the heating and heat transfer process during the welding. The results are obtained in the form of Models and corresponding graphs. The temperature color scale for all results ranges from Blue, for minimum temperature, to Red, for maximum temperature, as shown in Figure 15. The simulation indicates that increasing the friction time will leads to an increasing in the temperature beyond the melting point of the stainless-steel. This means that increasing the friction time might lead to thin molten layers of metal between the faces in contact, even if this type of welding in considered a non-melting weld. Figure 12 shows the generating of heat between the rubbed faces and Figure 13 shows the temperature distribution for one halve of the heated joint. The temperature keeps increasing with time and does not stop at the melting point of stainless-steel, $1400 - 1450$ °C. At t=11.5*sec*, layers of both halves reach a temperature of approximately 2990 °C; hence, molten layers of metal is presented between the two faces in contact.
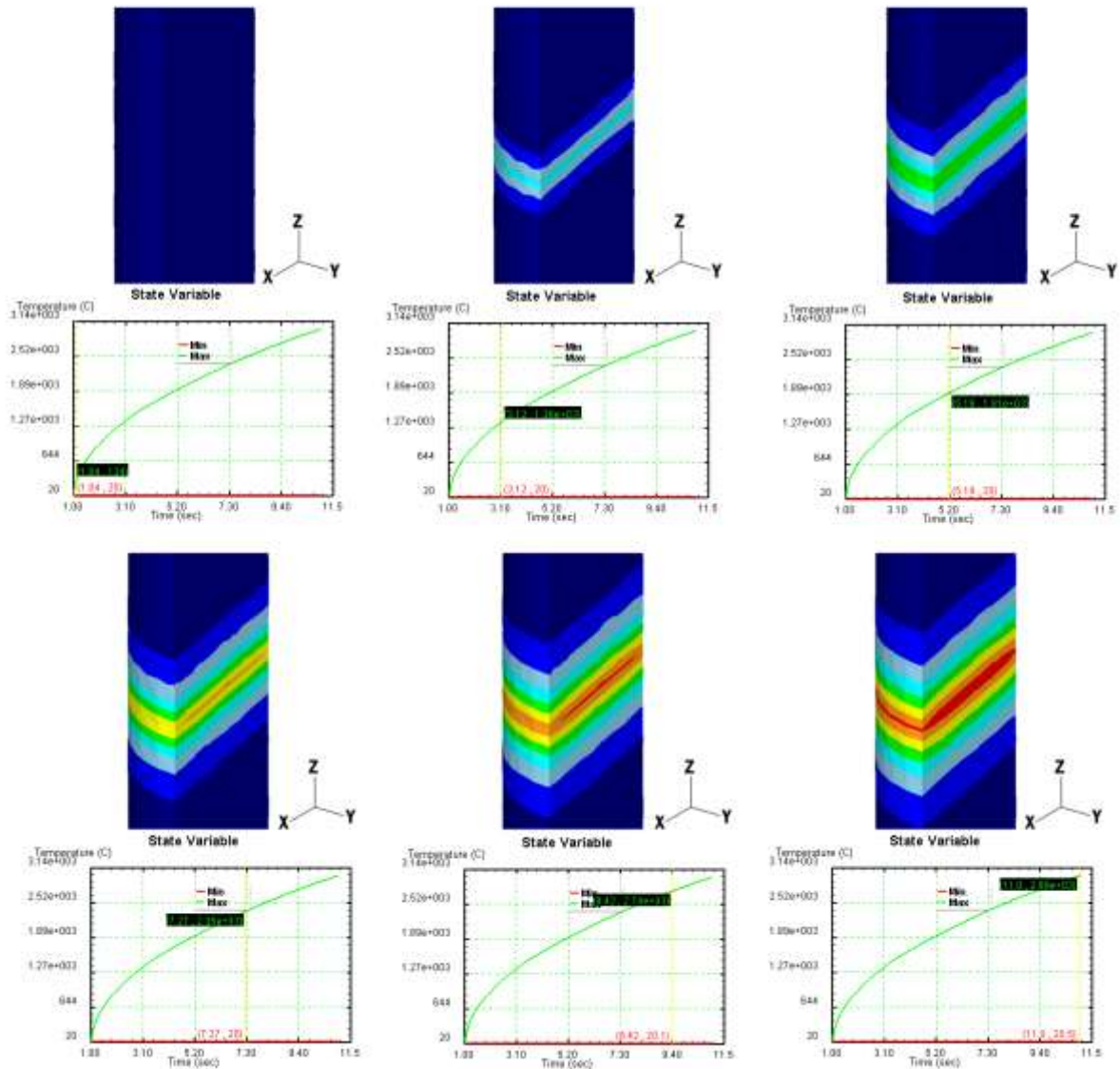
Figure 12: Frictional heating simulation results (Both Halves, Isometric Section View), the corresponding time for each view is marked on the diagrams with a vertical yellow line.

Figure 14 shows the radial temperature distribution across the rubbed face on one halve, the same behaviour is expected or the opposite face. Each 100 simulation step represents one second of friction heating and the distribution was sensed over 1000 point along the radius, indicated on the models by p1 − p1000 line. Initially, the maximum temperature is sensed at the outer point of the heated surface while the minimum temperature is sensed at the center of rotation; hence, the temperature distribution is directly proportional to the radial displacement. As the friction continues, the temperature distribution gradually oppose the initial state until, eventually, the maximum temperature is sensed at the center of rotation and the minimum temperature is sensed at the outer point of the heated surface; hence, the temperature distribution is inversely proportional to the radial displacement. This behaviour is due to the combined act of heat transfer and generated heat and it is divided into three stages, $T \propto R$, Intermediate and $T \frac{1}{\propto} R$ as follows:
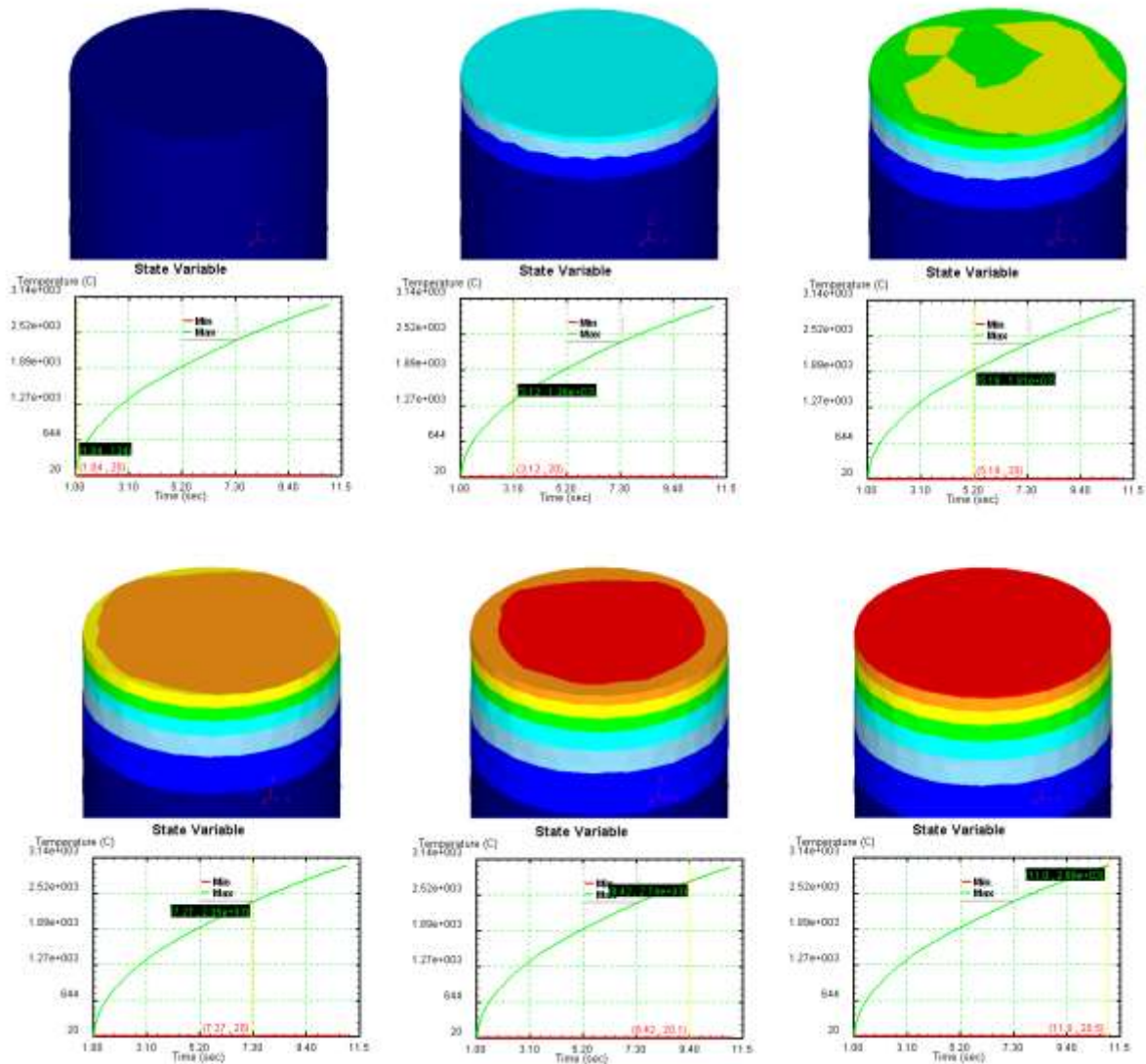
Figure 13: Frictional heating simulation results (One Halve, Isometric Top View), the corresponding time for each view is marked on the diagrams with a vertical yellow line.

Stage I Initially, the heat generates from the friction between the two rubbed faces. As the frictional heat is directly proportional to the frictional speed, Maximum heat is generated at the outer perimeter, where the linear velocity is maximised, and Minimum heat is generated at the center of rotation, where ideally there is no linear velocity.

Stage II As the friction continues, heat is transferred from the perimeter zone toward the center of rotation by conduction, according to the second law of thermodynamics, and toward the surrounding environment by convection. This means that the center gains heat while the perimeter zone losses heat.

Stage III Continues heat loss and heat gain at different zone will reduce the sensed temperature of the perimeter and increase the sensed temperature of the center until the initial stages is opposed.

It should be noted that the third stage is to eventually change into a fourth stage of equilibrium, after welding, according to the laws of thermodynamics.

From the simulation results, a heating profile for stage III was generated, Figure 15. From the profile, the sensed temperature is maximized at the core of the welding area, the center of both halves. This profile also shows that

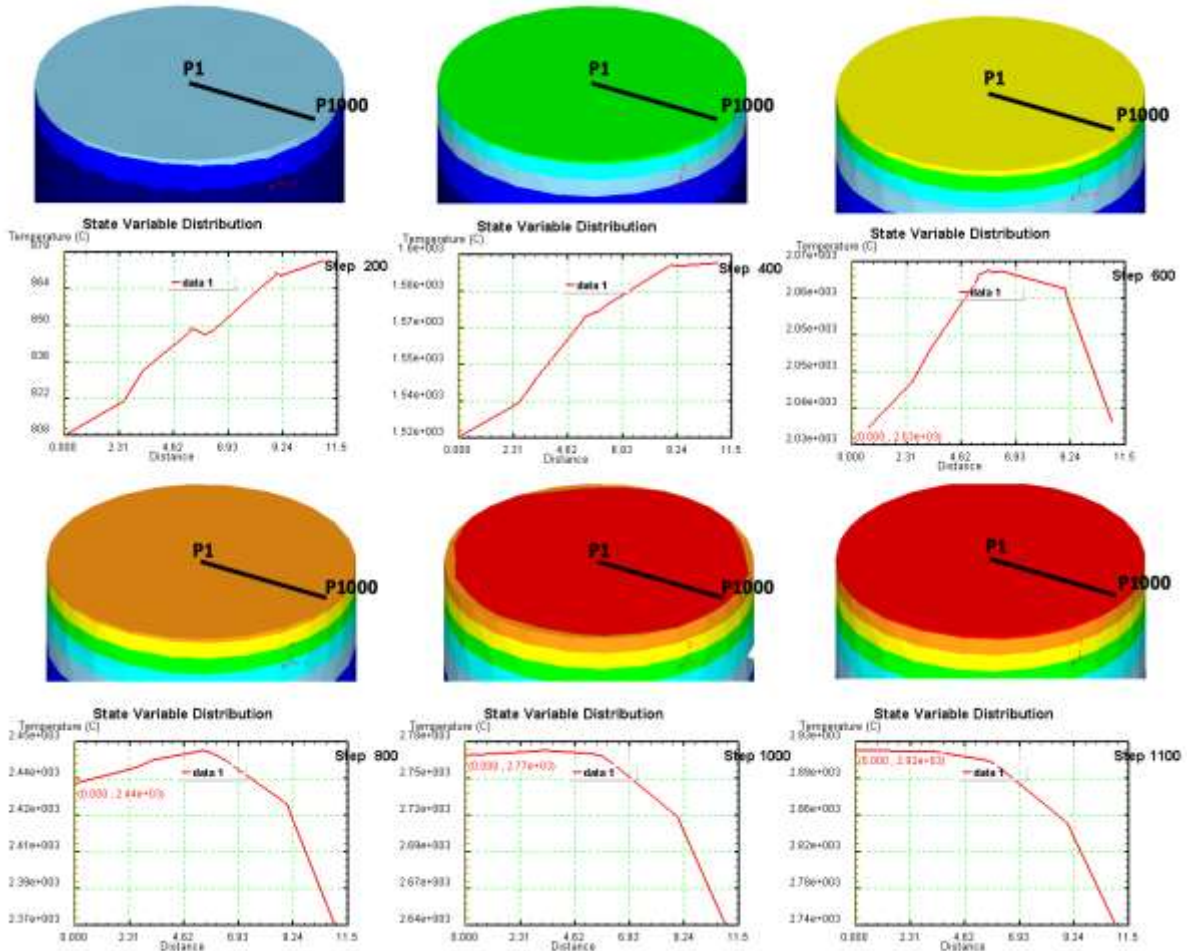the rate of heat transfer is directly proportional to the radius.

Figure 14: Frictional heating simulation results, Radial Distribution (One Halve, Isometric Top View), the corresponding graph for each view represents the temperature distribution across the indicated P1-P1000 line.
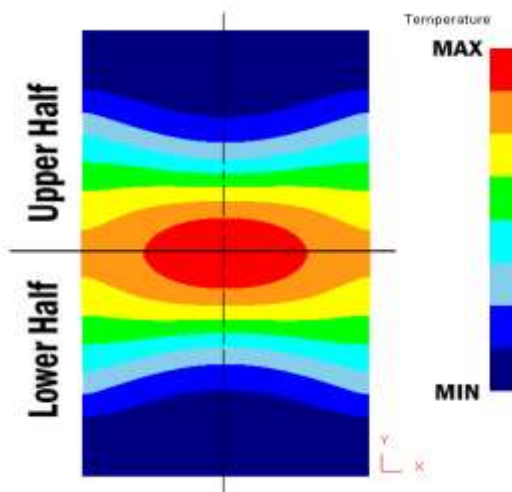

Figure 15: Frictional heating simulation results, Heating Profile (Both Halve, Front Section View)

CONCLUSION

This research investigated the effect of frictional welding between different stainless-steel materials on their Impact properties. The study was based on two main outcomes. The first was test results of specimens welded with different forging pressures. The second was the FEA of frictional heating process. Studying the obtained data, the following conclusions were reached:

1. The welded specimens were more brittle and less ductile. The amount of impact energy the specimens could withstand at the welded zone before fracture was, at the best, was 71.42% less than that of the non-welded specimens.
2. Increasing the forging pressure leads to an increasing in the carbon concentration which in terms reduces the ductility of the welded zone.
3. During continues friction, the temperature keeps increasing with time, leading to thin layers of molten metal between the rubbed faces, noting that the temperature does not reach the melting point of carbon.
4. The frictional heating profile of the dubbed faces has two main stages. At the first stage, the maximum temperature is sensed at the perimeter and the minimum temperature is sensed at the center. At the third stage, following an intermediate stage, the maximum temperature is sensed at the center and the minimum temperature is sensed at the perimeter.
5. The maximum heat transfer occurs at the perimeter of the welded joints, while the minimum heat transfer is found to be at the core of the welded joints.

REFERENCES

[1] Mmin AHN. Friction welding of different materials. INTERNATIONAL SCIENTIFIC CONFERENCE, 2010.
[2] Selim Sarper YILMAZ Mehmet UZKUT, Bekir Sadk NL and Mustafa AKDA. Friction welding and its applications in todays world. , .
[3] Friction Welding. MTI, 1999.
[4] Shubhavardhan RN and Surendran S. Friction welding to join dissimilar metals. International Journal of Emerging Technology and Advanced Engineering, 2012.
[5] S. B. DUNKERTON. Toughness properties of friction welds in steels. THE WELDING JOURNAL, 1986.
[6] Amit Handa and Vikas Chawla. Experimental evaluation of mechanical properties of friction welded aisi steels. Cogent Engineering, 2014.
[7] A.B. Ismail Uday M. Basheer, M.N. Ahmad Fauzi and H. Zuhailawati. Effect of friction time on the properties of friction welded ysz-alumina composite and 6061 aluminium alloy. Qatar Foundation Journals, 2013.
[8] Amit Handa and Vikas Chawla. An investigation on the effect of axial pressures on the mechanical properties of friction welded dissimilar steels. Advances in Mechanical Engineering, 2014.
[9] Joshua M. Duell. Impact testing of advanced composites. , .
[10] Yamin Shaoa Omar Fergani and Steven Y. Liang. Effect of temperature on the subsurface microstructure and mechanical properties of aa 7075-t6 in machining. In 2nd CIRP 2nd CIRP Conference on Surface Integrity (CSI).
[11] V. A. Borisenko G. S. Pisarenko and Yu. A. Kashtalyan. The effect of temperature on the hardness and modulus of elasticity of tungsten and molybdenum. Poroshkovaya Metallurgiya, 1962.
[12] S. N. BAHADUR L.T. DWIVEDI H. D. MERCHANT, G. S. MURTY and Y. MEHROTRA. Hardness-temperature relationships in metals. JOURNAL OF MATERIALS SCIENCE, 1973.
[13] Ahmet CAN. Modelling of friction welding. INTERNATIONAL SCIENTIFIC CONFERENCE, 2010.
[14] Fengshou Gu Xiaocong He and Andrew Ball. A review of numerical analysis of friction stir welding. Progress in Materials Science, 2014.
[15] L. Y. DUAN BY L. FU and S. G. DU. Numerical simulation of inertia friction welding process by finite element method. WELDING JOURNAL, 2003.
[16] BY R. L. KLUEH and D. P. EDMONDS. Chemical composition effects on the creep strength of type 308 stainless steel weld metal. THE WELDING JOURNAL, 1986.
[17] BY R. L. KLUEH and D. P. EDMONDS. Chemical composition effects on the creep of type 316 and 16-8-2 stainless steel weld metal. THE WELDING JOURNAL, 1986. Figure 12: Frictional heating simulation results (Both Halves, Isometric Section View)